ARCHIVES OF ELECTRICAL ENGINEERING VOL. 67(2), pp. 391–402 (2018)

DOI 10.24425/119648

# Parameters identification of coreless axial flux permanent magnet generator

NATALIA RADWAN-PRAGŁOWSKA, TOMASZ WĘGIEL, DARIUSZ BORKOWSKI

*Cracow University of Technology*
*e-mail: natalia.radwan-praglowska@pk.edu.pl*

(Received: 30.11.2017, revised: 16.03.2018)

**Abstract:** This paper presents an analytical model of a three-phase axial flux coreless generator excited by permanent magnets, with special focus on determining the model parameters. An important aspect of this model is the derivation of a coefficient that corrects the flux on the inside and outside edges of the magnets. The obtained parameters are verified by performing field analyses and measurements. A comparison of the results show satisfactory convergence, which confirms the accuracy of the proposed analytical model.

**Key words:** axial flux generator, permanent magnets

## 1. Introduction

In recent years, there have been reports on improved techniques for the design and mathematical modelling of permanent magnet (PM) machines [1–8]. The simplest models of traditional machines are based on the distribution of the air-gap field radial component because of the specific structure of the magnetic circuit. The geometry of the magnetic circuit in the axial flux permanent magnet (AFPM) machine is different compared with that of classical machines, and the relations which describe the flux-density distribution used for modelling should therefore be modified. Over the years, several AFPM machines have been developed, and a number of different topologies can be distinguished [5].

This work focuses primarily on AFPM generators (AFPMGs) with a coreless stator (Fig. 1) and winding topology of non-overlapping windings [5–8]. Such designs are commonly performed in a crude manner. While AFPM generators with coreless stators are mainly used in small, domestic wind-power plants, they have some disadvantages. These include the formation of very large attractive forces between the disks of the rotor with a relatively large volume related to the obtained power. Obvious advantages are that there is no formation of cogging torque and the design simplicity. Therefore, this paper aims to show the methodology of mathematical modelling for a specific AFPMG class.

The main assumption of AFPMG modelling is its simplicity. The main goal was to refer to traditional electrical machines models as well as to consider the effect of the interaction of higher harmonics of the flux-density distribution on the shape of the electromotive force (EMF).

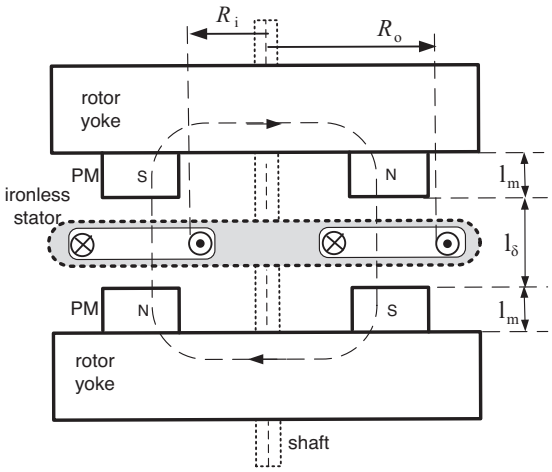


Fig. 1. Construction of dual-rotor AFPM generator

## 2. Analytical model of 3-phase coreless AFPM generator

### 2.1. Flux-density distribution in AFPM generator air gap

The main features of the AFPM generator are presented in Table 1. For this example, the analytical formula which describes the magnetic-field distribution in the machine air gap was developed.

Table 1. Main features of machine construction with non-overlapping windings

| | |
|---|---|
| Number of phase coils | $p_s$ |
| Total number of stator coils | $3p_s$ |
| Number of magnets (one rotor side) | $4p_s = 2p$ |
| $p/p_s$ | 2 |
| Maximal angle of coil pitch | $\varepsilon_{max} = \dfrac{2\pi}{3p_s} = \dfrac{4\pi}{3p}$ |

For the AFPM generator, the authors made an assumption concerning the linear approximation for the PM demagnetization characteristics $B_m = B_r + \mu_0 \cdot \mu_{rm} \cdot H_m$ (where: $B_r$ is the magnet remanence, $\mu_{rm}$ is the relative magnet permeability), and neglecting the magnetic voltage drops in iron. The main elements of the AFPMG are shown in Fig. 2.

To illustrate the methodology of the field distribution in the air gap, the authors used the coordinates model, which depicts the AFPM machine, as shown in Fig. 3.

The model of the magnetic-field distribution in the air gap of the AFPM machine is generally a function of four variables (dependent on the axial coordinate $z$, the location according to the stator $\theta$, the angle of the rotor position $\varphi$ and the radial location $R_i \leq r \leq R_o$). In the paper,

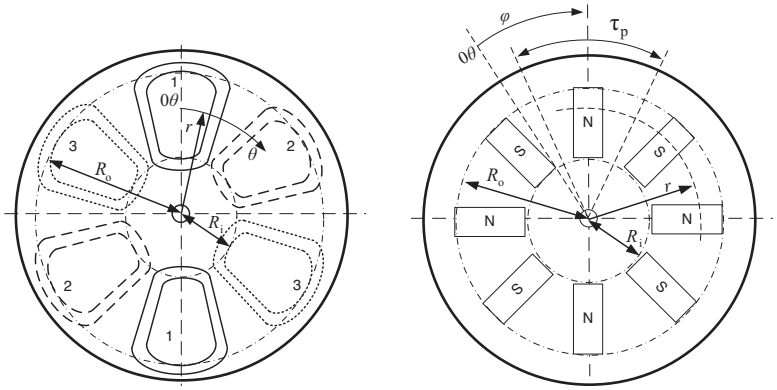


Fig. 2. Cross-section of AFPM generator: (a) stator (3-phase non-overlapping winding $p_s = 2$); (b) one of rotor discs ($p = 4$)

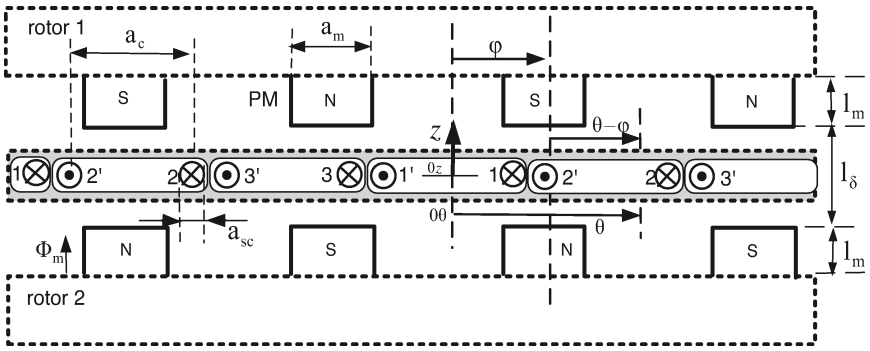


Fig. 3. Model of coordinate system for flux-density distribution

the general formula which represents the magnetic flux density is simplified, and only the axial component at the coordinate $z = 0$ is considered.

$$B(z=0,\theta,\varphi,r) = B(\theta,\varphi,r) = B_\Theta(\theta,r) + B_\mathrm{m}(\theta-\varphi,r), \tag{1}$$

where: $B_\Theta(\theta,r)$ is the axial component of the flux density induced by the winding magnetomotive forces (MMFs) at $z = 0$, and $B_\mathrm{m}(\theta-\varphi,r)$ is the PM axial component of the flux density at $z = 0$.

The MMF component describes the field distribution, which is dependent on the winding currents. The 3-phase AFPM machines with a symmetrical structure (the layouts of the stator windings are shown in Fig. 4) can be presented in the following form [9, 10, 11]:

$$B_\Theta(\theta,r) = \lambda_0 \cdot \sum_{a=1}^{3} \Theta_a(\theta,r), \tag{2}$$

where $\lambda_0$ is the unit permeance and $\Theta_a(\theta,r)$ is the function of the MMF of winding "$a$".

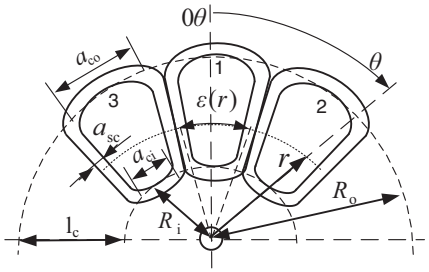


Fig. 4. Layout of non-overlapping winding type

The unit permeance, which is due to the properties of the magnet being similar to those of air ($\mu_{\mathrm{rm}} \cong 1.01, \cdots, 1.1$), is virtually constant.

$$\lambda_0 = \frac{\mu_0}{\mathrm{l}_\delta + 2\mathrm{l}'_{\mathrm{m}}}, \tag{3}$$

where $\mathrm{l}'_{\mathrm{m}} = \dfrac{\mathrm{l}_{\mathrm{m}}}{\mu_{\mathrm{rm}}}$, $\mathrm{l}_{\mathrm{m}}$ is the magnet height and $\mathrm{l}_\delta$ is the length of the equivalent air gap.

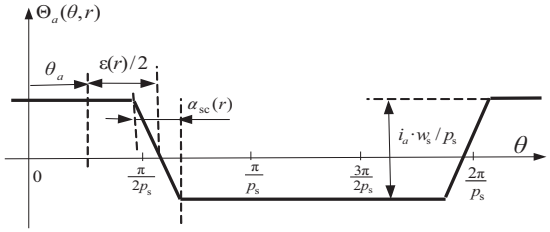


Fig. 5. Winding "*a*" MMF distribution

The Fourier distribution of the MMF of winding "*a*" (Fig. 5) is represented by the following formula:

$$\Theta_a(\theta, r) = \sum_{\nu \in P} \Theta^a_\nu(r) \cdot \mathrm{e}^{\mathrm{j}\nu(\theta - \theta_a)}, \tag{4}$$

where the Fourier spectra of the MMFs contain harmonics of the $\nu^{\mathrm{th}}$ order, which belongs to the set $P = \{\ldots, -3p_{\mathrm{s}}, -2p_{\mathrm{s}}, -p_{\mathrm{s}}, p_{\mathrm{s}}, 2p_{\mathrm{s}}, 3p_{\mathrm{s}}, \ldots\}$.

$$\Theta^a_\nu(r) = i_a \frac{1}{\pi} W^{\mathrm{s}}_\nu(r), \tag{5}$$

$$W^{\mathrm{s}}_\nu(r) = \frac{w_{\mathrm{s}} \cdot k^{|\nu|}_{\mathrm{s}}(r)}{|\nu|}, \tag{6}$$

$w_{\mathrm{s}}$ is the total number of phase winding turns, $k^{|\nu|}_{\mathrm{s}}(r)$ is the winding factor for $\nu^{\mathrm{th}}$ harmonic.

For the 3-phase winding $\theta_a = (a-1)\dfrac{2\pi}{3p_s}$, where $a = 1, 2, 3$.

For concentrated coils, the winding factor can be written as [5]:

$$k_s^{|\nu|}(r) = \sin\left(|\nu|\frac{\varepsilon(r)}{2}\right) \cdot \frac{\sin\left(|\nu|\dfrac{\alpha_{sc}(r)}{2}\right)}{|\nu|\dfrac{\alpha_{sc}(r)}{2}}, \tag{7}$$

where $\varepsilon(r) = \dfrac{a_c}{r}$ is the angle of the coil pitch or coil span at coordinate $r$ $\left(a_c \approx \dfrac{a_{co}+a_{ci}}{2}\right)$, and $\alpha_{sc}(r) = \dfrac{a_{sc}}{r}$ is the angle of the coil side width at coordinate $r$.

An approximation of the axial component of the PM flux density in the middle of the air gap (coordinate $z = 0$) for the AFPM machines (the layout of the rotor is shown in Fig. 6) is presented in Fig. 7.

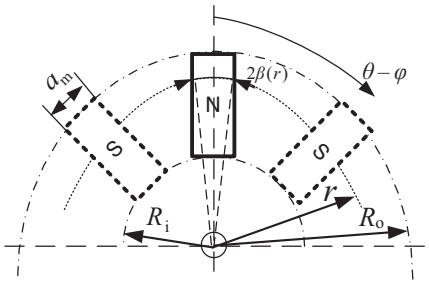


Fig. 6. Layouts of exemplary PM shapes located on the rotor

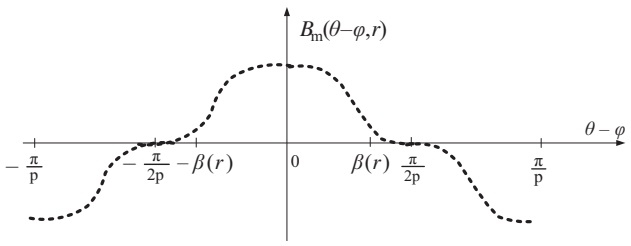


Fig. 7. Approximated functions of PM axial flux-density distribution in air gap according to coordinate $\theta - \varphi$

The Fourier series coefficients of the PM flux-density distribution (Fig. 7) can be determined from the following formula [7, 11–13]:

$$B_m(\theta-\varphi, r) = \sum_{\varsigma \in Q} B_\varsigma^{PM}(r) \cdot e^{j\varsigma(\theta-\varphi)}, \tag{8}$$

where the Fourier spectra contain harmonics of the $\varsigma^{th}$ order, which belongs to the set $Q = \{\ldots\ -5p, -3p, -p, p, 3p, 5p\ \ldots\}$. Fourier coefficients $B_\varsigma^{PM}(r)$ can be determined using

a one-dimensional (1D) model which is independent of the $z$ coordinate, and is sufficiently accurate for machines with small air gaps [11]. However, for AFPM coreless generators, the two-dimensional (2D) model is more appropriate, which is dependent on the $z$ coordinate where it is assumed that $z = 0$ [12, 13].

$$B_{\varsigma}^{\mathrm{PM}}(r) = \frac{4B_{\mathrm{r}}}{\pi}\frac{p}{\varsigma}\cdot\sin(\varsigma\cdot\beta(r))\frac{\sinh\left(|\varsigma|\dfrac{\mathrm{l_m}}{r}\right)}{\mu_{\mathrm{rm}}\cdot\sinh\left(|\varsigma|\dfrac{\mathrm{l}_\delta+2\mathrm{l_m}}{r}\right)}\cdot \cdot\left[\cosh\left(|\varsigma|\frac{\frac{\mathrm{l}_\delta}{2}+\mathrm{l_m}-z}{r}\right)+\cosh\left(|\varsigma|\frac{\frac{\mathrm{l}_\delta}{2}+\mathrm{l_m}+z}{r}\right)\right], \tag{9}$$

where

$$\beta(r) = \frac{a_{\mathrm{m}}}{2r}. \tag{10}$$

$\beta(r)$ is the half angular pitch of the magnet pole at coordinate $r$ $\left(a_{\mathrm{m}} \approx \dfrac{a_{\mathrm{mo}}+a_{\mathrm{mi}}}{2}\right)$.

## 3. Mathematical model of AFPM generator

Using Lagrange's formalism to develop the mathematical model, the AFPM generator equations can be written in a standard matrix form, according to [10, 11], as follows:

$$\frac{\mathrm{d}}{\mathrm{d}t}\begin{bmatrix}\psi_{\mathrm{PM1}}(\varphi)\\ \psi_{\mathrm{PM2}}(\varphi)\\ \psi_{\mathrm{PM3}}(\varphi)\end{bmatrix} = \begin{bmatrix}u_1\\ u_2\\ u_3\end{bmatrix} + \begin{bmatrix}L_{\sigma\mathrm{s}}+L_{\mathrm{ss}} & M_{\sigma\mathrm{s}} & M_{\sigma\mathrm{s}}\\ M_{\sigma\mathrm{s}} & L_{\sigma\mathrm{s}}+L_{\mathrm{ss}} & M_{\sigma\mathrm{s}}\\ M_{\sigma\mathrm{s}} & M_{\sigma\mathrm{s}} & L_{\sigma\mathrm{s}}+L_{\mathrm{ss}}\end{bmatrix}\cdot\frac{\mathrm{d}}{\mathrm{d}t}\begin{bmatrix}i_1\\ i_2\\ i_3\end{bmatrix} + R_{\mathrm{s}}\cdot\begin{bmatrix}i_1\\ i_2\\ i_3\end{bmatrix}, \tag{11}$$

$$J\frac{\mathrm{d}^2\varphi}{\mathrm{d}t^2} = T_{\mathrm{L}} - \begin{bmatrix}i_1 & i_2 & i_3\end{bmatrix}\cdot\frac{\partial}{\partial\varphi}\begin{bmatrix}\psi_{\mathrm{PM1}}(\varphi)\\ \psi_{\mathrm{PM2}}(\varphi)\\ \psi_{\mathrm{PM3}}(\varphi)\end{bmatrix} - D\frac{\mathrm{d}\varphi}{\mathrm{d}t}. \tag{12}$$

In order to determine the basic parameters of the mathematical model of the generator (11), (12) the flux linked with windings has to be defined. The flux, $\psi_a$, which is linked with the "$a$" winding, can be expressed as:

$$\psi_a(\varphi) = \int_{R_i}^{R_{\mathrm{o}}} w_{\mathrm{s}}\left\{\int_{\frac{-\varepsilon(r)+\alpha_{\mathrm{sc}}(r)}{2}+\theta_a}^{\frac{\varepsilon(r)-\alpha_{\mathrm{sc}}(r)}{2}+\theta_a} B(\theta,\varphi,r)\,\mathrm{d}\theta\right\} r\,\mathrm{d}r. \tag{13}$$

For the assumed flux-density distribution, $B(\theta,\varphi,r)$, integrations in Expression (13) are tedious. However, they are simplified under the assumption which introduces an average value

$$r \approx r_{\mathrm{s}} = \frac{R_{\mathrm{o}}+R_i}{2}. \tag{14}$$

The "$a$" winding's flux linkage, $\psi_{\mathrm{PM}a}$, which is generated by magnets in the current-less state, is represented by the classical relationship

$$\psi_{\mathrm{PM}a}(\varphi) = \sum_{\varsigma \in Q} \psi_{\varsigma}^{\mathrm{PMs}} \cdot \mathrm{e}^{\mathrm{j}\varsigma\left\{(a-1)\frac{4\pi}{3p}-\varphi\right\}} \quad \text{for } a = 1,\ 2,\ 3. \tag{15}$$

The coefficients of the function distribution of the stator flux PM linkage (15) have to be modified in order to model the flux attenuation on the magnet edges. This correction is important for the quantitative analysis because of the relatively large air gap in the studied generator construction with coreless stator. By introducing the flux-density distribution in the 2D air gap according to (9), (10), it is possible to model the effects on the magnet edges (along coordinate $r$). A separate problem is the implementation of the PM flux attenuation on the edges which are perpendicular to coordinate $r$, that is, the inside (for $r = R_i$) and outside (for $r = R_{\mathrm{o}}$) edges of PM. The analytical formulas enable us to determine whether the edge effects are complex [7, 12, 13]. The approximated flux-density distribution generated by magnets in the middle of the air gap, $z = 0$, along the radial coordinate is presented in Fig. 8.

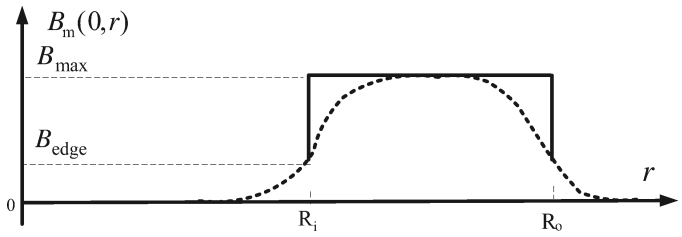


Fig. 8. Approximated functions of PM axial flux-density distribution in the middle of the air gap ($z = 0$) according to coordinate $r$ for $\theta - \varphi = 0$

This paper proposes to determine the correction coefficient $k_{\mathrm{e}}$ which models the flux attenuation on the inside and outside magnet edges using characteristic parameters $B_{\mathrm{edge}}/B_{\max}$ determined from field analysis. The parameters are presented in Fig. 8. The value of these parameters can be calculated as a ratio of the average value of the sinusoidal approximation of the step function (solid line in Fig. 8) within the range $(R_i, R_{\mathrm{o}})$ to the maximal value. The coefficient can be found as follows:

$$k_{\mathrm{e}} = \frac{\frac{4}{\pi}(B_{\max} - B_{\mathrm{edge}})\frac{2}{\pi} + B_{\mathrm{edge}}}{B_{\max}}. \tag{16}$$

The corrected form of the function distribution coefficients (15) is given below:

$$\psi_{\varsigma}^{\mathrm{PMs}} = 2k_{\mathrm{e}} \cdot B_{\varsigma}^{\mathrm{PM}}(r_{\mathrm{s}}) \cdot W_{\varsigma}^{\mathrm{s}}(r_{\mathrm{s}}) \cdot r_{\mathrm{s}} \cdot \mathrm{l_c}, \tag{17}$$

where $\mathrm{l_c} = R_{\mathrm{o}} - R_i$ is the length of the coil side.

The EMF of the '$a$' winding generated by magnets in a current-less state for a constant rotary speed is given by

$$e_{\mathrm{PM}a} = \sum_{\varsigma = p, 3p, 5p\ldots} E_{\varsigma} \cdot \cos\varsigma\left\{\Omega t - (a-1)\frac{4\pi}{3p}\right\} \quad \text{for } a = 1,\ 2,\ 3, \tag{18}$$

where $E_{\varsigma} = 2\varsigma\,\Omega\,\psi_{\varsigma}^{\mathrm{PMs}}$ and $\Omega$ is the rotary speed (rad/s).

After completion of the formal mathematical operations, the winding inductances are represented by the standard general dependence [10, 11]

$$L_{\mathrm{ss}} = \sum_{\nu \in P} L_{\nu}^{\mathrm{ss}}, \qquad L_{\nu}^{\mathrm{ss}} = \frac{2}{\pi} \cdot [W_{\nu}^{\mathrm{s}}(r_{\mathrm{s}})]^2 \cdot r_{\mathrm{s}} \cdot \mathrm{l_c} \cdot \lambda_0 \,. \tag{19}$$

The leakage inductances are expressed analytically as a sum of two components [5]. One of them is connected with the leakage flux around the radial portions of the active conductors (corresponding to the slot leakage in classical machines), and the second is dependent on the leakage flux around the coil end connections. The leakage inductance coefficient can be determined from the following formula:

$$L_{\sigma \mathrm{s}} \approx 2\mu_0 \cdot (w_{\mathrm{s}})^2 [\mathrm{l_c} + (a_{\mathrm{c}} - a_{\mathrm{sc}})] \cdot 0.3/p_{\mathrm{s}} \,. \tag{20}$$

Equations (19), (20) can yield approximated results; therefore, for some cases, it is necessary to apply the FEM calculations in order to achieve correct results [14]. The leakage mutual inductances can be approximated to zero $M_{\sigma \mathrm{s}} \approx 0$.

## 4. Experimental results

The tests were carried out for the 3-phase AFPM generator constructed under workshop conditions. The design data and parameters are summarized in Table 2.

Table 2. The main data of AFPM generator

| | |
|---|---|
| Number of phase coils $p_{\mathrm{s}} = 7$ | Number of pole pairs $p = 14$ |
| Total number of stator coils $= 21$ | Total number of phase winding turns $w_{\mathrm{s}} = 980$ |
| Stator coil dimensions<br>$\mathrm{l_c} = 40$ mm; $a_{\mathrm{c}} = 50$ mm; $a_{\mathrm{sc}} = 30$ mm | Length of equivalent air gap $\mathrm{l}_{\delta} = 26$ mm |
| $R_i = 270$ mm | $R_{\mathrm{o}} = 310$ mm |
| $r_{\mathrm{s}} = 290$ mm | Phase winding resistance $R_{\mathrm{s}} = 2.0\ \Omega$ |
| Angle of coil side width $\alpha_{\mathrm{sc}}(r_{\mathrm{s}}) = 0.1034$ rad | Angle of coil pitch $\varepsilon(r_{\mathrm{s}}) = 0.1517$ rad |
| Magnet size (type N40)<br>$B_{\mathrm{r}} = 1.2$ T, $H_{\mathrm{c}} = 899$ kA/m, $\mu_{\mathrm{rm}} = 1.07$,<br>$10 \times 18 \times 40$ mm; $a_{\mathrm{m}} = 18$ mm; $\mathrm{l_m} = 10$ mm | Number of magnets (one rotor side) $2p = 28$<br>Half-angular pitch of magnet pole<br>$\beta(r_{\mathrm{s}}) = 0.0345$ rad |

The view of the stator and rotor before assembling the AFPM generator, and the assembled generator installed in a lab station is presented in Fig. 9.

To assess the usefulness of analytical formulas, the calculations in the field package ANSYS-Maxwell (FEM – 3D) were performed. The layouts of the FEM model are presented in Fig. 10.

Based on the results obtained from the FEM calculations, the main flux values were separated from the leakage flux, and this enabled us to perform the inductance calculations. The comparison of the analytical calculations with the results obtained from the FEM is presented in Table 3.

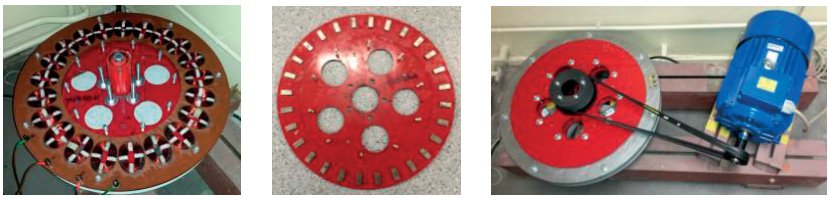

(a) (b) (c)

Fig. 9. AFPM generator: (a) stator; (b) rotor (one side); (c) at the laboratory test bench

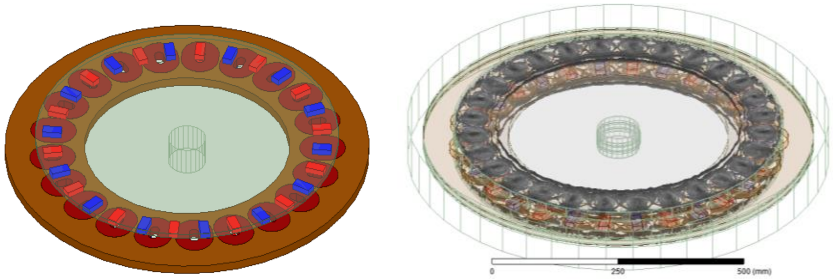

Fig. 10. AFPMG model for FEM calculations

Table 3. Inductances of AFPM generator

| **Inductances** | $L_{\sigma s}$ | $M_{\sigma s}$ | $L_{ss}$ |
|---|---|---|---|
| **Analytical formulas** | 6.2 mH | 0 | 4.0 mH |
| **FEM calculations** | 5.12 mH | −0.009 mH | 4.1 mH |

The analysis of results from Table 3 show a satisfactory correctness of the results obtained using the analytical formulas. The values of the leakage inductances differ themselves by around 20% owing to the simplified analytical Formula (20).

In the next step, the functions of the PM axial flux-density distribution in the air gap according to coordinate $\theta - \varphi$ in the middle of air gap (coordinate $z = 0$) obtained using analytical formula and FEM analysis were calculated. The results are presented in Figs 11, 12.

From Fig. 11, it is seen that the PM axial flux-density distributions in the middle of the air gap are almost identical. However, the distributions differ significantly for different values of radial coordinate $r$, which is shown in Fig. 12.

The characteristic parameters, which equal $B_{\text{edge}}/B_{\text{max}} = 0.16/0.29$ (taken from Fig. 12), allow us to determine the coefficient that models the PM edge effects on the inside and outside sides of the magnet. The value of this coefficient equals $k_{\text{e}} = 0.93$, and it is used in analytical calculations of phase back EMF (19).

The time-domain waveforms of EMF voltages and the spectrum analysis are presented in Figs 13, 14. The voltage level at 1 mV was chosen as a reference for the magnitude presentation (in dB).

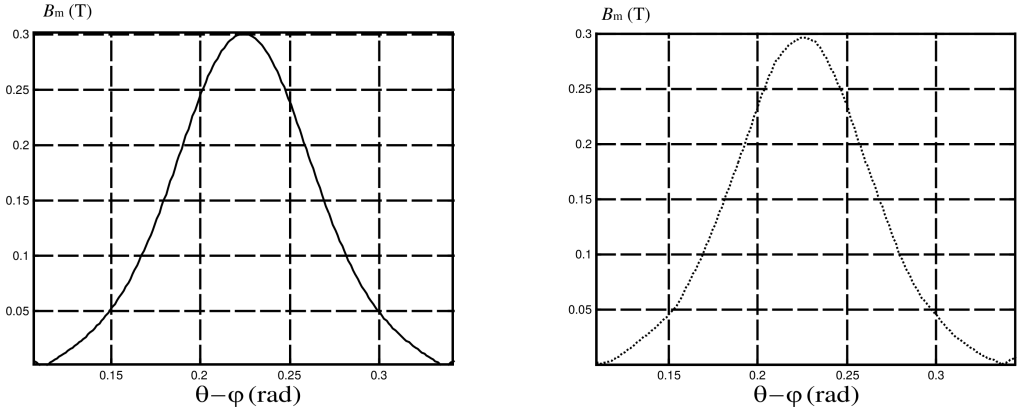


Fig. 11. Functions of PM axial flux density distribution in the middle of air gap $B_{\mathrm{m}}(\theta-\varphi, r_{\mathrm{s}})$ for one pole pitch: (a) solid line – analytical formula; (b) dashed line – FEM calculations)

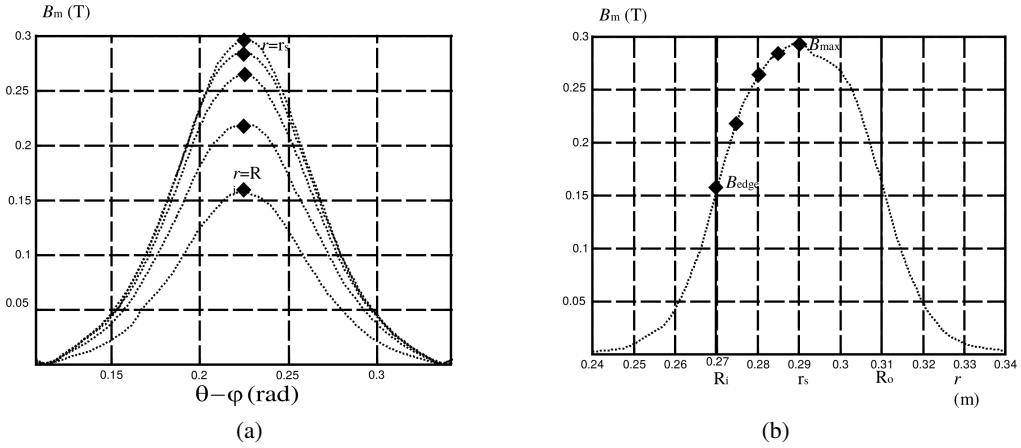


Fig. 12. FEM calculations of PM axial flux density distribution in middle of air gap: (a) $B_{\mathrm{m}}(\theta-\varphi, r)$ for one pole pitch and different values of coordinate $r$; (b) $B_{\mathrm{m}}(\theta-\varphi=0.225=\mathrm{const}, r)$ according to coordinate $r$

By observing the voltage waveforms from Fig. 13, the deformation of the induced EMF waveform from a sine wave can be determined. The RMS values and THD of the back EMF at rotary speed $n = 206$ rpm ($f = 48$ Hz) are: analytical calculations 61.1 V (THD 6.1%); measurements 61.8 V (THD 8.4%) and FEM calculations 64.4 V (THD 6.2%). These values vary by about 10%. By analysing the amplitude values obtained from Fig. 14, a significant content of the third harmonic and a minor part of the fifth harmonic in the back EMF can be observed. These results confirm good agreement between the measurements and calculations.

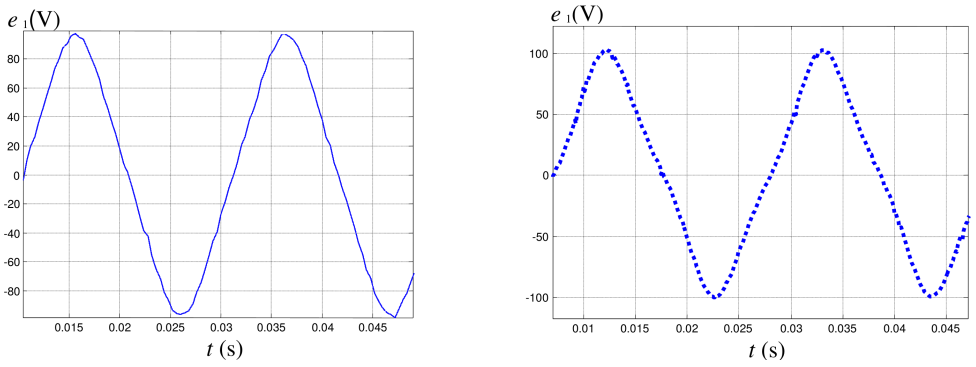


Fig. 13. Phase-1 back EMF at rotary speed $n = 206$ rpm ($f = 48$ Hz): (a) FEM calculations; (b) measured

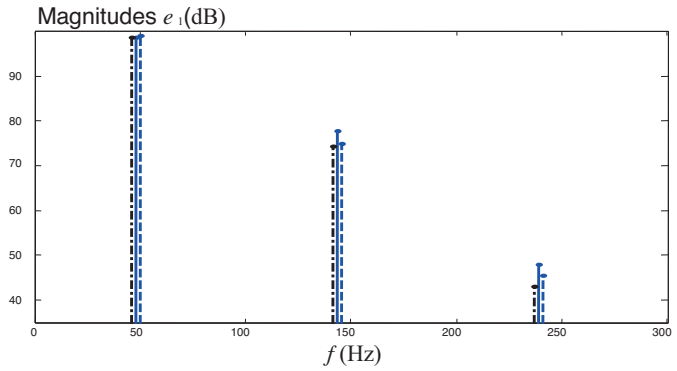


Fig. 14. Comparisons of phase back EMF magnitudes at rotary speed $n = 206$ rpm ($f = 48$ Hz): dash-dot line – computed analytically; solid line – measurement results and dashed line – FEM calculations

## 5. Conclusions

This paper presents the methodology employed for the development of circuit models of the 3-phase AFPM generator. The laboratory tests and FEM analysis, which verify the mathematical model parameters obtained using the basic analytical formulas, are presented. The good agreement of the analytical calculation with the measurement results and FEM calculations confirms the correctness of the developed models. It should be noted that there is perfect agreement between the results from analytical calculation and field analysis.

**Acknowledgements**

This work was supported by the Polish Ministry of Science and Higher Education under grant no. E-2/605/2017/DS-M.

**References**


[1] Wojciechowski R.M., *Analysis and optimisation of an axial flux permanent magnet coreless motor based on the field model using the superposition principle and genetic algorithm*, Archives of Electrical Engineering, vol. 65, no. 3, pp. 601–611 (2016).

[2] Paplicki P., *Modified concept of axial-flux permanent magnet machine with field weakening capability*, Archives of Electrical Engineering, vol. 63, no. 2, pp. 177–185 (2014).

[3] Borkowski D., Węgiel T., *Small hydropower plant with integrated turbine-generators working at variable speed*, IEEE Transaction of Energy Conversion, vol. 28, no. 2, pp. 452–459 (2013).

[4] Mazgaj W., Szular Z., Węgiel T., Sobczyk T., *Small hydropower plant with variable speed PM generator*, Przegląd Elektrotechniczny, R. 87, no. 5, pp. 282–287 (2011).

[5] Gieras J., Wang R., Kamper M., *Axial flux permanent magnet brushless machines*, Kluwer Academic Publishers (2004).

[6] Kamper M.J., Wang R.-J., Rossouw F.G., *Analysis and performance of axial flux permanent-magnet machine with air-cored nonoverlapping concentrated stator windings*, IEEE Transactions on Industry Applications, vol. 44, iss. 5, pp. 1495–1504 (2008).

[7] Choi J.Y., Lee S.H., Ko K.J., Jang S.M., *Improved analytical model for electromagnetic analysis of axial flux machines with double-sided permanent magnet rotor and coreless stator windings*, IEEE Trans. on Magnetics, vol. 47, no. 10, pp. 2760–2763 (2011).

[8] Kanuch J., Ferkova Z., *Design and simulation of disk stepper motor with permanent magnets*, Archives of Electrical Engineering, vol. 62, no. 2, pp. 281–288 (2013).

[9] Zhu Z.Q., Howe D., Ekkehard B., Ackermann B., *Instantaneous magnetic field distribution in brushless permanent magnet motors, part I: Open-circuit field*, IEEE Trans. Magn., vol. 29, pp. 124–134 (1993).

[10] Węgiel T., *Space harmonic interactions in permanent magnet generator*, Wydawnictwo Politechniki Krakowskiej, Monograph 447, ISSN 0860-097X, Cracow (2013).

[11] Węgiel T., *Space harmonic interactions in axial flux permanent magnet generator*, Technical Transactions, Electrical Engeenering 2-E, pp. 65–79 (2016).

[12] Zhilichev Y.N., *Three-dimensional analytic model of permanent magnet axial flux machine*, IEEE Trans. Magn., vol. 34, no. 6, pp. 3897–3901 (1998).

[13] Azzouzi J., Barakat G., Dayko B., *Quasi-3D analytical modeling of the magnetic field of an axial flux permanent-magnet synchronous machine*, IEEE Trans. on Energy Conversion, vol. 20, no. 4, pp. 746–752 (2005).

[14] Demenko A., Nowak L., Pietrowski W., *Calculation of magnetization characteristic of a squirrel cage machine using edge element*, The international journal for computation and mathematics in electrical and electronic engineering, vol. 23, no. 4, pp. 1110–1118 (2004).